Appl. Math. Mech. -Engl. Ed., **42**(7), 1047–1062 (2021)

APPLIED MATHEMATICS AND MECHANICS (ENGLISH EDITION)

https://doi.org/10.1007/s10483-021-2752-6

Heat transfer analysis of MHD and electroosmotic flow of non-Newtonian fluid in a rotating microfluidic channel: an exact solution*

T. SIVA[1], S. JANGILI[2,†], B. KUMBHAKAR[1]

1. Department of Mathematics, National Institute of Technology Meghalaya, Shillong 793003, India;
2. Department of Mathematics, National Institute of Technology Warangal, Telangana 506004, India

(Received Mar. 4, 2021 / Revised May 17, 2021)

Abstract The heat transfer of the combined magnetohydrodynamic (MHD) and electroosmotic flow (EOF) of non-Newtonian fluid in a rotating microchannel is analyzed. A couple stress fluid model is scrutinized to simulate the rheological characteristics of the fluid. The exact solution for the energy transport equation is achieved. Subsequently, this solution is utilized to obtain the flow velocity and volume flow rates within the flow domain under appropriate boundary conditions. The obtained analytical solution results are compared with the previous data in the literature, and good agreement is obtained. A detailed parametric study of the effects of several factors, e.g., the rotational Reynolds number, the Joule heating parameter, the couple stress parameter, the Hartmann number, and the buoyancy parameter, on the flow velocities and temperature is explored. It is unveiled that the elevation in a couple stress parameter enhances the EOF velocity in the axial direction.

Key words microfluidic, electric double layer (EDL), electroosmotic flow (EOF), magnetohydrodynamic (MHD), couple stress fluid

Chinese Library Classification O357.1, O351.2, O363.2
2010 Mathematics Subject Classification 76W05, 76A05, 76U05

1 Introduction

Recently, microfluidic transport processes have attracted the attention of engineers due to their prevalent applications in vast fields, e.g., micro-electro-mechanical systems (MEMS), chemical separation equipments, biomedical diagnostic techniques, thermal management of microelectronic systems, biochemical engineering, cell retrieval processes, drug delivery biochip, and particle sorting[1–5]. These applications may allow a broad range of operations, e.g., transportation of bio-chemical and physiological fluids (blood, DNA solution, saliva, etc.), actuation

* Citation: SIVA, T., JANGILI, S., and KUMBHAKAR, B. Heat transfer analysis of MHD and electroosmotic flow of non-Newtonian fluid in a rotating microfluidic channel: an exact solution. *Applied Mathematics and Mechanics* (*English Edition*), **42**(7), 1047–1062 (2021) https://doi.org/10.1007/s10483-021-2752-6

† Corresponding author, E-mail: jsrinivas@nitw.ac.in

and tool detection, and separation of species[6–7]. According to the electrostatic theory, the essential thermo-chemical interaction between the microflow device/system charged boundary and the electrolyte solution develops a particular charge distribution, including both the Stern and diffuse layers. The combination of both the sub-layers represents the electric double layer (EDL), which usually forms at the boundary of the solid-liquid interface. Subsequently, a fluid flow takes place inside the EDL due to the applied electric body force known as electroosmotic flow (EOF)[8].

Rotating nano/microfluidic platforms have many vital applications such as drug development and point-of-care medical diagnostics[6,9]. Chang and Wang[10] studied the EOF of Newtonian fluid through a rotating parallel plate-channel for the first time, developed exact solutions for the velocity distribution and flow rates, and observed that the transverse velocity existed due to the Coriolis force. Subsequently, several studies were carried out on the EOFs of Newtonian fluid[11–12] and non-Newtonian fluid (e.g., viscoelastic fluid[13], power-law fluid[14], Maxwell fluid[15], third-grade fluid[16], Eyring fluid[17], and couple stress fluid[18]) in rotational microchannels. Some other related works pertaining to various geometrical configurations have also been reported[19–22].

The study of fluid flow and thermal analysis in rotating microchannels with the electric and magnetic field combination has gained significant consideration due to its sundry applications in engineering and manufacturing systems, e.g., heat exchangers and cooling of electronic devices. Researchers have recently observed that the imposed magnetic field can effectively reduce the Joule heating effect compared with purely electroosmotic force. It was also identified that the mixed MHD and EOF effects could improve the fluid flow rates in microchannels[23].

In many practical engineering applications, internal heat generation might create a serious problem compared with EOFs because of the significant side effects of the temperature rise in the microfluidic systems. Therefore, the thermal control of microscale and nanoscale devices has become more critical and challenging due to the rapid extraction of heat in microchannels. Heat transfer analysis is important in microfluidics at microscale, e.g., electronic device cooling[24] and microchannel heat sink[25]. The first study on fully developed EOF thermal properties in microchannels was carried out by Maynes and Webb[26]. They obtained a closed-form expression for the temperature distribution by considering the Debye-Hückel approximation. Furthermore, it was observed that the Joule heating parameter decreased the Nusselt number variation. Horiuchi and Dutta[27] extended Maynes and Webb's work. They considered the Joule heating effects on the thermal analysis of the EOF in a microchannel, and obtained an analytical solution of the thermal field of a microchannel by using the separation-of-variable method. Numerous works have been reported in the literature with the consideration of non-Newtonian fluid models of thermal properties on EOF by using different configurations[28–30].

The theory of traditional electrokinetic transport phenomena is dependent on the hypothesis that the fluid particles do not have any internal structures, e.g., Newtonian fluid. However, complex structure fluids such as polymer suspensions, liquid crystals, colloids, animal blood, lubricants, cell suspensions, chemicals, and drugs are often manipulated in microfluidic equipment. Couple stress fluids exhibit a prominent non-Newtonian behavior. In order to understand the characteristics of these fluids, researchers established several theories. The basic theory of microcontinua was developed by Stokes[31] at University of Delaware in 1966. Couple stress fluids consist of important material properties, which makes them different from classical viscous fluids. The couple stress fluid theory is the most straightforward generalization of the Newtonian viscous theory. It allows for polar effects such as couple stresses, body couples, and a non-symmetric stress tensor, and its rheological characteristics have many applications such as separation of crude oil from petroleum products and electrostatics precipitation[32]. Ariman and Cakmak[33] presented the analytical solutions of the Poiseuille and Couette flows by using micropolar and couple stress theories. The authors clearly explained the boundary conditions and their physical relevance in the context of these theories. Stokes[34] utilized his own model

to describe the effects of couple stresses on an MHD flow. The interested readers can refer to the excellent monograph on this theory in Ref. [35]. Recent modern technologies have led researchers to work on various problems. Devakar et al.[36] reported the analytical solutions of some fundamental flow problems such as simple Couette flow (purely shear driven flow), Poiseuille flow (purely pressure driven flow), and generalized Couette flow. However, these studies did not consider the electric field or electroosmotic effect on couple stress flows. The first such study was conducted by Tripathi et al.[37] who obtained an exact solution to describe the electric field as it could significantly enhance the transport rate in microfluidic devices. Later, Misra and Chandra[38] explored the bio-fluid EOF through a circular microchannel. Recently, Sinha et al.[39] performed a theoretical analysis on the heat transfer characteristics of EOF through a rotating porous microchannel, considering the slip velocity at the walls. They revealed that the blood flow in the rotating channel depended on the electroosmotic parameter and the slip parameter. Sun et al.[40] analyzed the rotating heat transfer and entropy of the viscous fluid EOF in a rectangular microchannel, and presented the heat transfer coefficient and entropy generation variations in detail for the first time with respect to several physical parameters.

Most of the works on the rotating heat transfer analyses of EOFs in the literature are reported for Newtonian fluid. In this analysis, we use the analytical method to inspect the steady MHD and EOF of a bio-fluid model in a rotating microfluidic channel by considering the slip condition at the wall. We obtain an exact solution to get the velocity and temperature variations inside the rotating microchannel. Then, we discuss the effects of several thermophysical parameters on the velocity, volume flow rates, and temperature distribution in detail. Our current work highlights the magnetic and electric force importance in enhancing the flow velocity and temperature distribution inside the microchannel. The present work has many important applications in biomedical engineering.

2 Mathematical formulation and geometry description

In this analysis, we consider the steady MHD and EOF of a couple stress fluid in a rotating microfluidic channel with a uniform temperature T_w at both porous walls (see Fig. 1). We adopt the coordinate system in such a way that its origin coincides with the center of the microfluidic channel with $2H$ being its height. The x'-axis is along the axial direction of the microchannel. The y'-axis is towards the outside of the plane. The z'-axis is perpendicular to the parallel plates. We assume that the fluid is injected consistently into the lower plate of

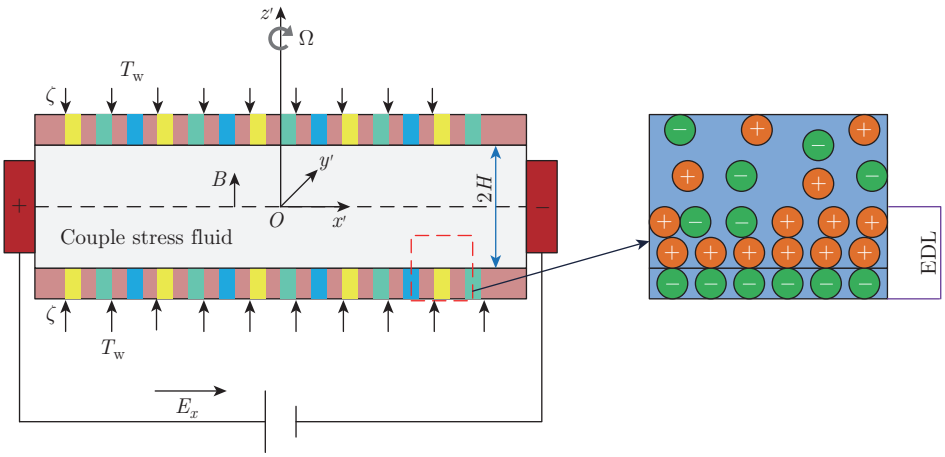

Fig. 1 Schematic sketch of the considered microfluidic channel (color online)

the microchannel, and suction occurs at the upper plate. We consider the couple stress fluid as an electrolyte solution in the rotating microchannel, which is uniformly charged with a zeta potential ζ at the porous walls. We adopt the Navier-slip condition at the channel boundaries. Further, we presume that the channel rotates about the z'-axis with a constant angular velocity $\boldsymbol{\Omega} = (0, 0, \Omega)$. The flow is driven by an applied external electric field $\boldsymbol{E} = (E_x,\, 0,\, 0)$ along the x'-axis. We assume that a constant and uniform magnetic field of the strength $\boldsymbol{B} = (0, 0, B_0)$ acts along the z'-axis.

2.1 Analysis of the EDL effects

Based on the electrostatic theory, the distribution of the net electric charge in the EDL can be represented by the Poisson equation[18,41] as follows:

$$\frac{\mathrm{d}^2\psi'}{\mathrm{d}z'^2} = -\frac{\rho_\mathrm{e}}{\varepsilon}, \tag{1}$$

where ψ' designates the electric potential, and ε represents the dielectric constant. The Boltzmann distribution for the charge density is given by

$$\rho_\mathrm{e} = -2n_0 z_0 e \sinh\Big(\frac{z_0 e}{k_\mathrm{B} T_\mathrm{ab}}\psi'\Big),$$

where n_0 is the bulk concentration of the ions, e is the electron charge, z_0 is the valence, k_B is the Boltzmann constant, and T_ab is the absolute temperature.

We consider the Boltzmann distribution of ions, and use the Debye-Hückel linear approximation (typically when $\psi' \leqslant 25\,\mathrm{mV}$) for the present transport process. The electrical potential distribution inside the EDL can be represented as the Poisson-Boltzmann equation as

$$\frac{\mathrm{d}^2\psi'}{\mathrm{d}z'^2} = \kappa^2\psi', \tag{2}$$

where $\kappa = \sqrt{\frac{2n_0 e^2 z_0^2}{\varepsilon k_\mathrm{B} T_\mathrm{ab}}}$ is the inverse of the Debye length. For getting the analytical expression of Eq. (2) in the desired direction of the channel, we consider the equivalent potential at the edges as follows:

$$\psi'|_{z'=\pm H} = \zeta. \tag{3}$$

To minimize the physical parameters in Eq. (2), we define the following non-dimensional quantities:

$$\psi = \psi'/\zeta, \quad z = z'/H, \quad K = H/\kappa^{-1}.$$

Then, the modified forms of Eqs. (2) and (3) are given by

$$\frac{\mathrm{d}^2\psi}{\mathrm{d}z^2} = K^2\psi, \tag{4}$$

$$\psi(z)|_{z=\pm 1} = 1. \tag{5}$$

With Eq. (5), the electrostatic potential distribution within the flow domain is obtained as

$$\psi(z) = \frac{\cosh(Kz)}{\cosh K}. \tag{6}$$

2.2 Analysis of the velocity and energy fields

The momentum and energy equations for the present investigation in a rotational environment are given by[39,42–43]

$$\upsilon_0 \frac{\mathrm{d}u'}{\mathrm{d}z'} - 2\Omega v' = \nu \frac{\mathrm{d}^2 u'}{\mathrm{d}z'^2} - \frac{\eta}{\rho}\frac{\mathrm{d}^4 u'}{\mathrm{d}z'^4} - \frac{\varepsilon E_x}{\rho}\frac{\mathrm{d}^2 \psi'}{\mathrm{d}z'^2} - \frac{\sigma {B_0}^2 u'}{\rho} + g\beta^*(T' - T_{\max}), \tag{7}$$

$$\upsilon_0 \frac{\mathrm{d}v'}{\mathrm{d}z'} + 2\Omega u' = \nu \frac{\mathrm{d}^2 v'}{\mathrm{d}z'^2} - \frac{\eta}{\rho}\frac{\mathrm{d}^4 v'}{\mathrm{d}z'^4} - \frac{\sigma {B_0}^2 v'}{\rho}, \tag{8}$$

$$\rho c_p \upsilon_0 \frac{\mathrm{d}T'}{\mathrm{d}z'} = k_f \frac{\mathrm{d}^2 T'}{\mathrm{d}z'^2} + \sigma E_x^2, \tag{9}$$

where u' and v' are the velocity components along the axial direction and the transverse direction, respectively. ρ is the density of the fluid. η is the couple stress viscosity coefficient. υ_0 is the suction/injection velocity in the z'-direction. g is the acceleration due to gravity. β^* is the thermal expansion coefficient. T' is the fluid temperature. $T_{\max}$ is the reference temperature. σ is the electrical conductivity. c_p is the specific heat at constant pressure. k_f is the thermal conductivity.

The terms $-2\Omega v'$ and $2\Omega u'$ appearing in Eqs. (7) and (8) are due to the rotational effects. The terms $-\frac{\varepsilon E_x}{\rho}\frac{\mathrm{d}^2\psi'}{\mathrm{d}z'^2}$, $-\frac{\sigma {B_0}^2 u'}{\rho}$, and $-\frac{\sigma {B_0}^2 v'}{\rho}$ in Eqs. (7) and (8), respectively, signify the effects of the applied electric force and the magnetic force in the axial and transverse directions. The penultimate term $g\beta^*(T' - T_{\max})$ in Eq. (7) signifies the body force due to thermal convection. The term σE_x^2 in Eq. (9) characterizes the Joule heating effect. We adopt the following boundary conditions for the present analysis[18,44–45]:

$$\left(u' + \beta_1' \frac{\mathrm{d}u'}{\mathrm{d}z'}\right)\bigg|_{z'=H} = 0, \quad \left(v' + \beta_1' \frac{\mathrm{d}v'}{\mathrm{d}z'}\right)\bigg|_{z'=H} = 0, \tag{10}$$

$$\left(u' - \beta_2' \frac{\mathrm{d}u'}{\mathrm{d}z'}\right)\bigg|_{z'=-H} = 0, \quad \left(v' - \beta_2' \frac{\mathrm{d}v'}{\mathrm{d}z'}\right)\bigg|_{z'=-H} = 0, \tag{11}$$

$$\left.\frac{\mathrm{d}^2 u'}{\mathrm{d}z'^2}\right|_{z'=\pm H} = \left.\frac{\mathrm{d}^2 v'}{\mathrm{d}z'^2}\right|_{z'=\pm H} = 0, \tag{12}$$

$$T'|_{z'=H} = T_{\mathrm{w}}, \quad \left.\frac{\mathrm{d}T'}{\mathrm{d}z'}\right|_{z'=0} = 0, \tag{13}$$

where β_1' and β_2' are the slip coefficients at the upper and lower walls, respectively. We define the following non-dimensional variables for describing the physical problem into a minimum number of quantities:

$$\begin{cases} u = \dfrac{u'}{U_{HS}}, \quad v = \dfrac{v'}{U_{HS}}, \\ T = \dfrac{T' - T_{\max}}{T_{\mathrm{w}} - T_{\max}}, \quad \beta_1 = \dfrac{\beta_1'}{H}, \quad \beta_2 = \dfrac{\beta_2'}{H}, \end{cases}$$

where β_1 and β_2 are the slip parameters at the top and bottom walls, respectively. T is the non-dimensional temperature. U_{HS} is the reference EOF velocity, and $U_{HS} = -\frac{\varepsilon E_x \zeta}{\mu}$.

Therefore, the dimensionless governing equations take the following forms:

$$\frac{\mathrm{d}^4u}{\mathrm{d}z^4}-\gamma^2\frac{\mathrm{d}^2u}{\mathrm{d}z^2}+SRe\gamma^2\frac{\mathrm{d}u}{\mathrm{d}z}-2\omega\gamma^2v+Ha^2\gamma^2u=K^2\gamma^2\psi+\lambda\gamma^2T, \tag{14}$$

$$\frac{\mathrm{d}^4v}{\mathrm{d}z^4}-\gamma^2\frac{\mathrm{d}^2v}{\mathrm{d}z^2}+SRe\gamma^2\frac{\mathrm{d}v}{\mathrm{d}z}+2\omega\gamma^2u+Ha^2\gamma^2v=0, \tag{15}$$

$$\frac{\mathrm{d}^2T}{\mathrm{d}z^2}-SRePr\frac{\mathrm{d}T}{\mathrm{d}z}=-J. \tag{16}$$

To find the solution of the system of Eqs. (14) and (15), we consider the special type of complex function transformation $\chi(z)=u(z)+\mathrm{i}v(z)$ in this analysis.

Therefore, Eqs. (14) and (15) and the respective boundary conditions take the following forms:

$$\frac{\mathrm{d}^4\chi}{\mathrm{d}z^4}-\gamma^2\frac{\mathrm{d}^2\chi}{\mathrm{d}z^2}+SRe\gamma^2\frac{\mathrm{d}\chi}{\mathrm{d}z}+\gamma^2(2\omega\mathrm{i}+Ha^2)\chi=K^2\gamma^2\frac{\cosh(Kz)}{\cosh K}+\lambda\gamma^2T, \tag{17}$$

$$\left(\chi+\beta_1\frac{\mathrm{d}\chi}{\mathrm{d}z}\right)\Big|_{z=1}=0,\quad \left(\chi-\beta_2\frac{\mathrm{d}\chi}{\mathrm{d}z}\right)\Big|_{z=-1}=0, \tag{18}$$

$$\frac{\mathrm{d}^2\chi}{\mathrm{d}z^2}\Big|_{z=\pm1}=0,\quad T|_{z=1}=1,\quad \frac{\mathrm{d}T}{\mathrm{d}z}\Big|_{z=0}=0, \tag{19}$$

where

$$\begin{cases} S=\dfrac{\upsilon_0}{U_{HS}},\quad Re=\dfrac{U_{HS}H}{\nu},\quad \gamma=\sqrt{\dfrac{\mu}{\eta}}H,\quad \omega=\dfrac{\Omega\eta^2}{\nu},\\[2ex] Ha=\sqrt{\dfrac{\sigma}{\mu}}B_0H,\quad Gr=\dfrac{g\beta^*H^3(T_{\mathrm{w}}-T_{\max})}{\nu^2},\quad \lambda=\dfrac{Gr}{Re}. \end{cases}$$

In the above equations, S is the suction parameter, Re is the Reynolds number, γ is the couple stress parameter[18,31,46], ω is the rotating Reynolds number in which ν is the kinematic viscosity[10,18,47], Ha is the Hartmann number, Gr is the Grashof number, λ is the buoyancy parameter, J is the Joule heating parameter, and Pr is the Prandtl number.

Therefore, the analytical solutions of the temperature distribution (see Eq. (16)) and velocity (see Eq. (17)) under the preceding boundary conditions are given by

$$T(z)=C_1+C_2\mathrm{e}^{\delta z}+\frac{J}{\delta}z, \tag{20}$$

$$\begin{aligned}\chi(z)={}&C_3\mathrm{e}^{-\alpha_1z}+C_4\mathrm{e}^{-\alpha_2z}+C_5\mathrm{e}^{\alpha_3z}+C_6\mathrm{e}^{\alpha_4z}\\&+\frac{K^2A}{2\cosh K}\Big(\frac{\mathrm{e}^{Kz}}{K^4-AK^2+BK+C}+\frac{\mathrm{e}^{-Kz}}{K^4-AK^2-BK+C}\Big)\\&+\frac{\lambda AC_1}{C}+\frac{\lambda AC_2}{\delta^4-A\delta^2+B\delta+C}\mathrm{e}^{\delta z}+\frac{\lambda AJ}{\delta C}\Big(z-\frac{B}{C}\Big),\end{aligned} \tag{21}$$

where the algebraic representations of C_3, C_4, C_5, and C_6 are very lengthy, and

$$\begin{cases} \delta = SRePr, \quad A = \gamma^2, \quad B = SReA, \quad C = A(2\omega \mathrm{i} + Ha^2), \quad C_1 = 1 - \dfrac{J}{\delta} + \dfrac{J}{\delta^2}\mathrm{e}^{\delta}, \\ C_2 = -\dfrac{J}{\delta^2}, \quad J = \dfrac{\sigma E_x^2 H^2}{k_f(T_{\mathrm{w}} - T_{\max})}, \quad Pr = \dfrac{\mu c_p}{k_f}, \quad \alpha_1 = \sigma_3 + \sigma_2, \\ \alpha_2 = \sigma_3 - \sigma_2, \quad \alpha_3 = \sigma_3 - \sigma_1, \quad \alpha_4 = \sigma_3 + \sigma_1, \\ \sigma_1 = \dfrac{(12A\sigma_6^{1/3}\sigma_5 - A^2\sigma_5 - 9\sigma_6^{2/3}\sigma_5 - 12C\sigma_5 - 3\sqrt{6}B\sqrt{3\sqrt{3}\sigma_7 - 2A^3 + 27B^2 + 72AC})^{1/2}}{\sigma_4}, \\ \sigma_2 = \dfrac{(12A\,\sigma_6^{1/3}\sigma_5 - A^2\sigma_5 - 9\,\sigma_6^{2/3}\sigma_5 - 12C\sigma_5 + 3\sqrt{6}B\sqrt{3\sqrt{3}\sigma_7 - 2A^3 + 27B^2 + 72AC})^{1/2}}{\sigma_4}, \\ \sigma_3 = \dfrac{\sigma_5}{6\sigma_6^{1/6}}, \quad \sigma_4 = 6\sigma_6^{1/6}(12C + 9\sigma_6^{2/3} + A^2 + 6A\sigma_6^{1/3})^{1/4}, \\ \sigma_5 = (12C + 9\sigma_6^{2/3} + A^2 + 6A\sigma_6^{1/3})^{1/2}, \quad \sigma_6 = \dfrac{\sqrt{3}\sigma_7}{18} - \dfrac{A^3}{27} + \dfrac{B^2}{2} + \dfrac{4AC}{3}, \\ \sigma_7 = (-16A^4C - 4A^3B^2 + 128A^2C^2 + 144AB^2C + 27B^4 - 256C^3)^{1/2}. \end{cases}$$

Nevertheless, here we do not include these constant values in the analysis for conciseness in the presentation.

The corresponding axial (Q_x) and transverse (Q_y) volume flow rates in the microchannel are

$$Q = Q_x + \mathrm{i}Q_y = \int_{-1}^{1} \chi \mathrm{d}z. \tag{22}$$

3 Results and discussion

3.1 Validation of the present model

To demonstrate the accuracy of the theoretical model in the current study, we compare the acquired analytical solution of the velocity distribution by considering $S = \lambda = Ha = 0$, $K = 10$, $\omega = 1$, and $\gamma = 140$ with the exact solution given by Chang and Wang[10] under the no-slip boundary condition ($\beta_1 = \beta_2 = 0$) for the rotating EOF between the parallel plates of the Newtonian fluid (see Fig. 2). It can be seen that the present results agree well with those in the literature. This validates that our analytical solution is effective and feasible.

3.2 Parameter selection

To describe the effects of the physical parameters on the EOF and heat transfer characteristics graphically, we choose the following values for the parameters obtained in the mathematical formulation. Based upon Refs. [39], [48], and [49], the typical values of the parameters considered in the present analysis are as follows:

$$\begin{cases} H \in [0\,\mu\mathrm{m}, 100\,\mu\mathrm{m}], \quad \mu = 3.2 \times 10^{-3}\,\mathrm{kg/(m \cdot s)}, \\ k_f = 2.2 \times 10^{-3}\,\mathrm{W/(m \cdot K)}, \quad c_p = 14.65\,\mathrm{J/(kg \cdot K)}, \\ B_0 \in [0.01\,\mathrm{T},\ 5\,\mathrm{T}], \quad \sigma \in [2.2 \times 10^{-4}\,\mathrm{S/m},\ 4 \times 10^{3}\,\mathrm{S/m}], \end{cases}$$

where H is the half-height of the microchannel, μ is the viscosity of the fluid, c_p is the specific heat at constant pressure, and B_0 is the magnetic field. The range of the electroosmotic parameter K is assumed to vary from 0 to 30 for the present study[6,10]. The buoyancy parameter

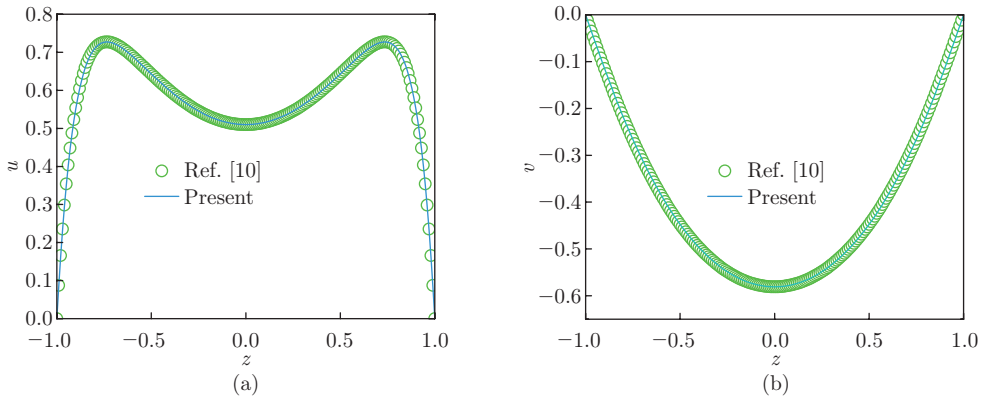

Fig. 2 Comparison of the present exact solution with the previously published theoretical result[10] (color online)

λ is taken to be of the order of 10[39,42]. The dimensionless Hartmann number Ha is between 0 and 0.5[47–48]. The dimensionless couple stress parameter γ varies from 0 and 10[18,46]. The dimensionless rotational speed ω varies from 0 to 5[18,47]. The Prandtl number Pr is between 20 and 25[39]. The Joule heating parameter J is from 0 to 0.5[39].

3.3 Effects of the couple stress parameter

In Fig. 3, we can observe the importance of the couple stress parameter γ on the flow velocity under the effects of both the electric field and the magnetic field. Figure 3(a) shows that the axial velocity distribution is enormously augmented by increasing the numeric values of γ. The effects of γ on the transverse velocity are plotted in Fig. 3(b). The increase in the transverse velocity is observed with increasing the values of γ. This may be due to the decrease in the values of the couple stress coefficient η as it decreases when γ increases. The further increase in γ indicates the decrease in the couple stress coefficient. When the couple stress coefficient η tends to zero (i.e., when the couple stresses are absent), Eqs. (7) and (8) reduce to the Navier-Stokes equation. Therefore, we can conclude that the absence of the couple stresses in the fluid medium enhances the flow velocity.

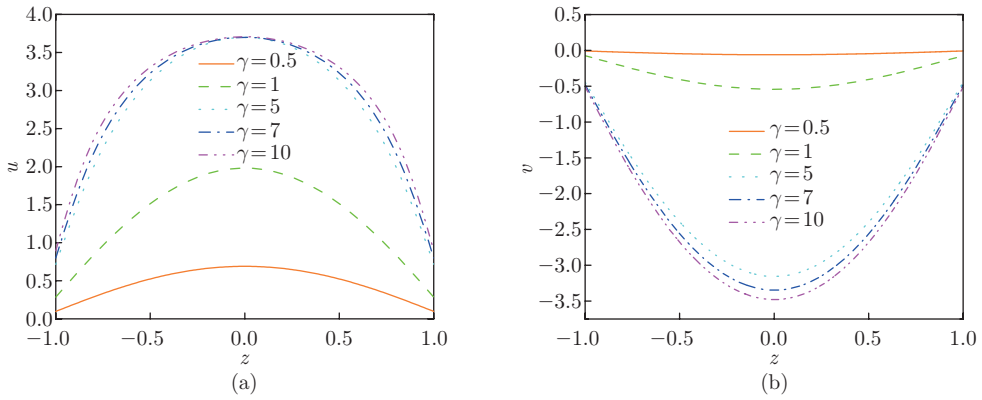

Fig. 3 Variations of the (a) u-axial and (b) v-transverse velocities for diverse values of γ when $\lambda = 10$, $Re = 0.01$, $S = 0.5$, $J = 0.1$, $Pr = 21$, $\omega = 1$, $K = 10$, $\beta_1 = \beta_2 = 0.1$, and $Ha = 0.5$ (color online)

3.4 Effects of the Hartmann number

Figure 4 illustrates the responses of the velocity distributions of the MHD and EOF for diverse values of the Hartmann number Ha. This number characterizes the ratio of the Lorentzian magnetic drag force (generated due to an interaction between the magnetic field induction and the electric current density) to the viscous force. It is witnessed from Fig. 4(a) that the fluid velocity diminishes with the increase in Ha in the axial direction. This is because of the magnetic force, which has a retarding effect on the primary flow velocity. Further, at higher Ha values, the reduction in the flow velocity is greater. Similar behavior can be seen in the secondary flow velocity with various Ha values, as demonstrated in Fig. 4(b). Overall, from Figs. 4(a) and 4(b), it is identified that the parameter Ha has a considerable retarding effect on the secondary flow as compared with the primary flow.

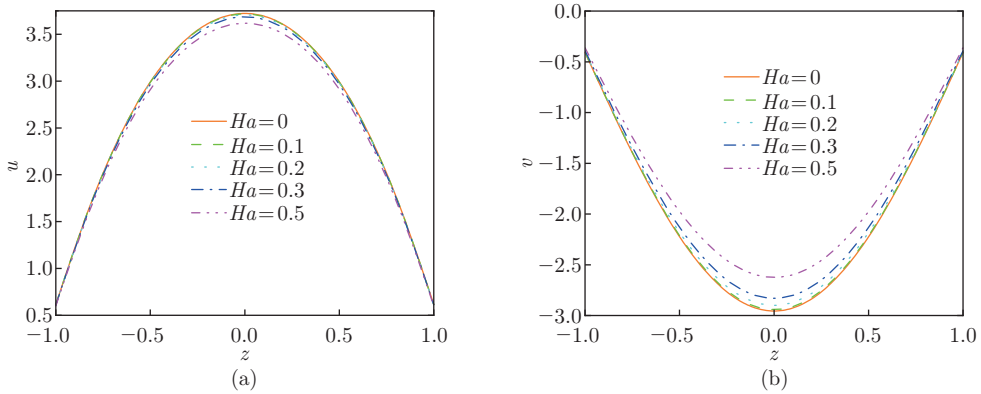

Fig. 4 Variations of the (a) u-axial and (b) v-transverse velocities for diverse values of Ha when $\lambda = 10$, $Re = 0.01$, $S = 0.5$, $J = 0.1$, $Pr = 21$, $\omega = 1$, $K = 10$, $\beta_1 = \beta_2 = 0.1$, and $\gamma = 3$ (color online)

3.5 Effects of the rotating fluid speed

One of the important parameters of the current work is the Coriolis force-based parameter, i.e., the rotating Reynolds number ω. Figure 5 highlights the variations of the axial and transverse velocity profiles for various values of ω $(= 0, 0.5, 1, 1.5, 2)$. From Fig. 5(a), it is perceived that the axial velocity diminishes across the microchannel, and it is parabolic in nature. Significantly, the profiles are constricted with the increase in the Coriolis force (higher values of ω). This decrease is mainly because the exchange of the streamwise flow strength drives the induced flow. This perception is compatible with the results published by Chang and Wang[10]. Next, it is noticed from Figs. 4(a) and 5(a) that the effects of the Coriolis force (when $1 < \omega < 2$) on the velocity are greater than those of the magnetic force. Conversely, the transverse velocity (see Fig. 5(a)) is increased (especially in the core-region) with the increase in ω. Further, a small change in the magnitude is noticed as compared with the axial velocity profiles. Overall, from Figs. 5(a) and 5(b), it is noticed that the effects of ω on the secondary flow are significant as compared with the primary flow.

3.6 Effects of the buoyancy parameter

The changes of the axial and transverse velocities concerning the buoyancy parameter λ can be seen in Fig. 6. This parameter signifies the relation between the temperature and velocity distributions. It is clearly identified from Figs. 6(a) and 6(b) that both the primary and induced velocity profiles consistently enhance with respect to λ. The physical meaning behind this is that the increase in λ is due to the differences of gravity and temperature between the channel walls. Also, it is noticed that the maximum velocity is attained in the core-region of the microchannel and the velocity profiles have a parabolic nature for higher values of λ.

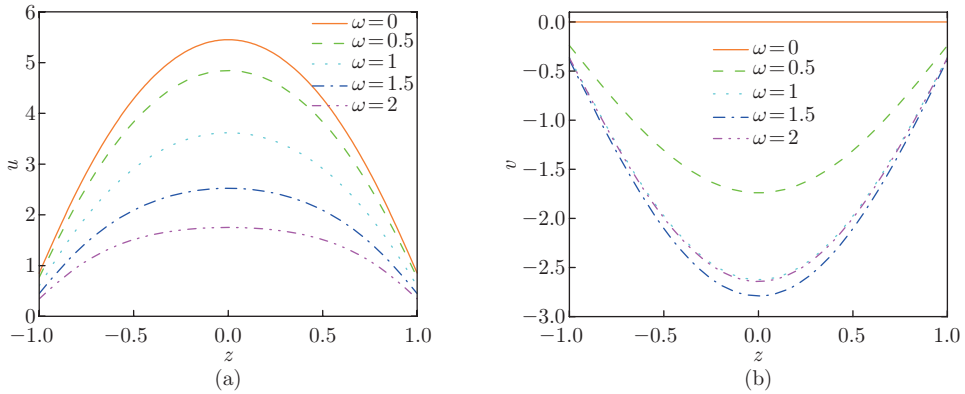

Fig. 5 Variations of the (a) u-axial and (b) v-transverse velocities for diverse values of ω when $\lambda = 10$, $Re = 0.01$, $S = 0.5$, $J = 0.1$, $Pr = 21$, $\gamma = 3$, $K = 10$, $\beta_1 = \beta_2 = 0.1$, and $Ha = 0.5$ (color online)

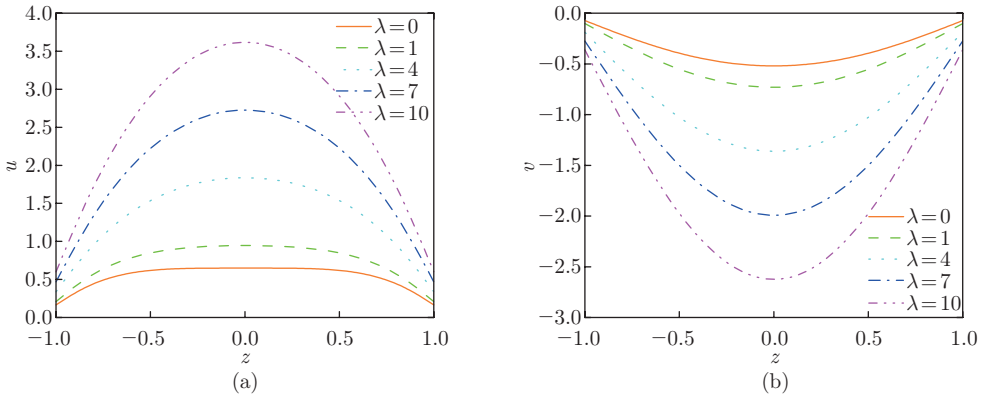

Fig. 6 Variations of the (a) u-axial and (b) v-transverse velocities for diverse values of λ when $Ha = 0.5$, $Re = 0.01$, $S = 0.5$, $J = 0.1$, $Pr = 21$, $\omega = 1$, $K = 10$, $\beta_1 = \beta_2 = 0.1$, and $\gamma = 3$ (color online)

3.7 Effects of the slip parameter at the top wall

Figure 7 shows the combined rotating MHD and EOF velocity variations for various values of the slip parameter β_1 at the top wall $z = 1$ of the microchannel. It is noticed from Figs. 7(a) and 7(b) that increasing the values of β_1 tends to elevate the mixed flow velocity in both directions. It may be mentioned here that the presence of a slip factor near the top wall of the microchannel has a potential effect on the flow velocity distribution of the EDL in the channel. The maximum velocity occurs due to the large substantial slip velocity. We can also observe that the streamwise velocity variation near the bottom wall ($z = -1$) is insignificant compared with the induced velocity variation at the same wall for several values of β_1. The presence of the slip velocity plays a prominent role in the transportation of ions inside the EDL. Also, the combination of the slip velocity and the EDL ion mobility plays a significant role in the energy transfer efficiency.

3.8 Effects of the slip parameter at the bottom wall

Figure 8 elucidates the combined rotating MHD and EOF velocity variations for various values of the slip parameter β_2 at $z = -1$ of the microchannel. It can be seen that the flow velocity modestly enhances when β_2 increases. The physical interpretation of Fig. 8 is the same

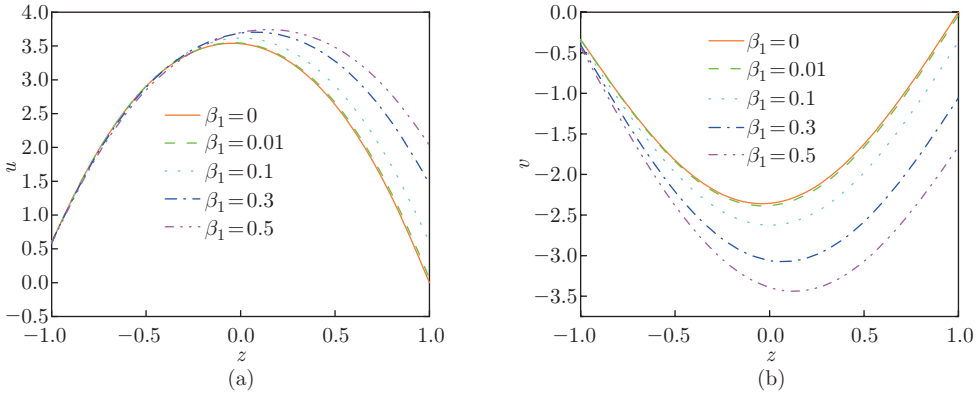

Fig. 7 Variations of the (a) u-axial and (b) v-transverse velocities for diverse values of β_1 when $Ha = 0.5$, $Re = 0.01$, $S = 0.5$, $J = 0.1$, $Pr = 21$, $\omega = 1$, $K = 10$, $\lambda = 10$, $\beta_2 = 0.1$, and $\gamma = 3$ (color online)

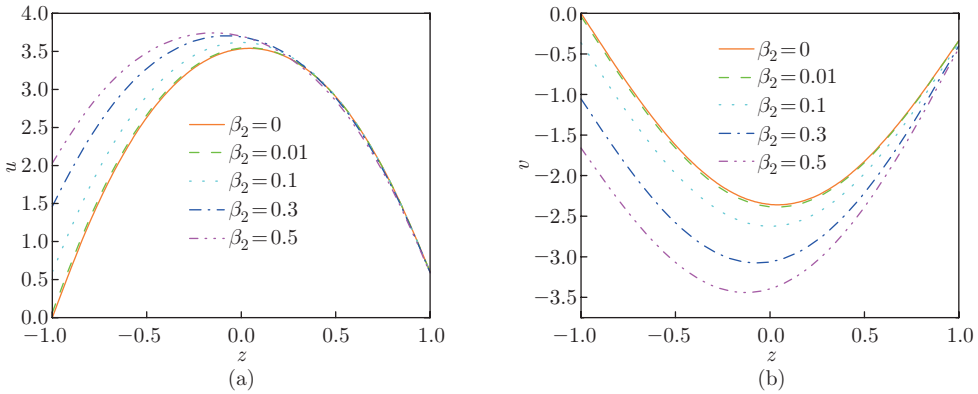

Fig. 8 Variations of the (a) u-axial and (b) v-transverse velocities for diverse values of β_2 when $Ha = 0.5$, $Re = 0.01$, $S = 0.5$, $J = 0.1$, $Pr = 21$, $\omega = 1$, $K = 10$, $\lambda = 10$, $\beta_1 = 0.1$, and $\gamma = 3$ (color online)

as that explored for the slip parameter β_1, but everything happens in reverse for β_2.

3.9 Variations of the volume flow rates in the microfluidic channel

One of the important quantities of interest in microchannel flow problems is the volume flow rates. Here, we attempt to describe the variations of the flow rates in the primary and secondary directions with increasing the values of ω.

Figure 9 elucidates the volume transport responses as a function of the electroosmotic parameter K for diverse values of ω. One may notice from Fig. 9(a) that the axial flow rate decreases with the increase in ω. Further, it is found that the flow rate achieves a steady behavior in the microchannel for large values of K. From Fig. 9(b), one can notice that the volume flow rate in the transverse direction increases when $\omega \leqslant 1.5$ and subsequently decreases when $\omega \geqslant 2$. Overall, from both the figures, it is perceived that the volume flow rate in the axial direction is larger than that in the transverse direction.

Now, we explain the effects of γ on the volume flow rates in both directions as shown in Figs. 10(a) and 10(b). It is more apparent from these plots that the volume flow rates increase when γ increases. A similar trend is found in the transverse direction. Overall, from Figs. 10(a) and 10(b), it is pointed out that γ has a retarding effect on the secondary flow as compared

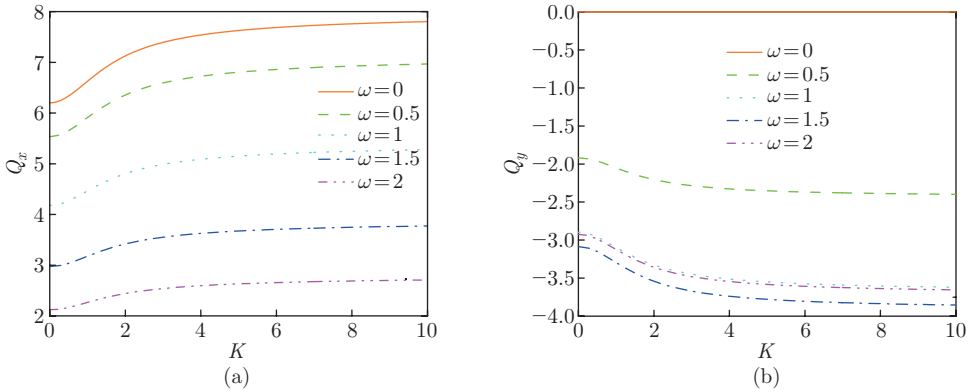

Fig. 9 Variations of the (a) Q_x-axial and (b) Q_y-transverse flow rates for diverse values of ω when $Ha = 0.5$, $Re = 0.01$, $S = 0.5$, $J = 0.1$, $Pr = 21$, $\lambda = 10$, $\beta_1 = \beta_2 = 0.1$, and $\gamma = 3$ (color online)

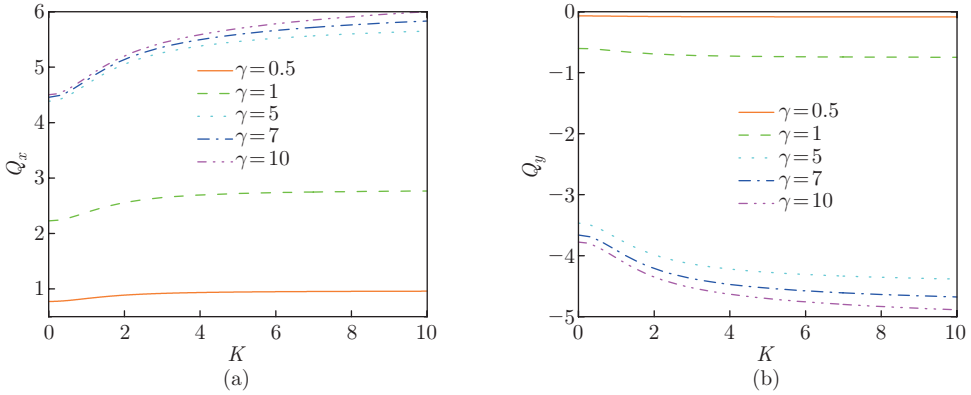

Fig. 10 Variations of the (a) Q_x-axial and (b) Q_y-transverse flow rates for diverse values of γ when $\omega = 1$, $Re = 0.01$, $S = 0.5$, $J = 0.1$, $Pr = 21$, $\lambda = 10$, $\beta_1 = \beta_2 = 0.1$, and $Ha = 0.5$ (color online)

with that on the primary flow. After examining the effects of ω and γ on the volume flow rates, we will highlight the effects of Ha on the axial and transverse flow rates.

Figures 11(a) and 11(b) show that both the flow rates decelerate as Ha increases.

From Figs. 9, 10, and 11, it is pointed out that the Hartmann number has a strong retarding effect on the control of the volume flow rates.

3.10 Thermal characteristics

After exploring the effects of several physical parameters on the MHD and EOF velocities and volume flow rates, we would like to describe the temperature distribution variations concerning Pr and J now. Figure 12 presents the thermal distribution depending on Pr. It is clearly understood from this figure that by increasing Pr, the temperature is increased. The physical meaning behind this is the rapid mobility of ions inside the channel due to the combined applied body forces from the magnetic and electric fields.

The responses of temperature for J are depicted in Fig. 13. It is clearly identified that the temperature distribution increases with the increase in J. This is because of high conductivity, which means that an external electric field is applied across the electrolyte solution, i.e., the couple stress fluid in the channel.

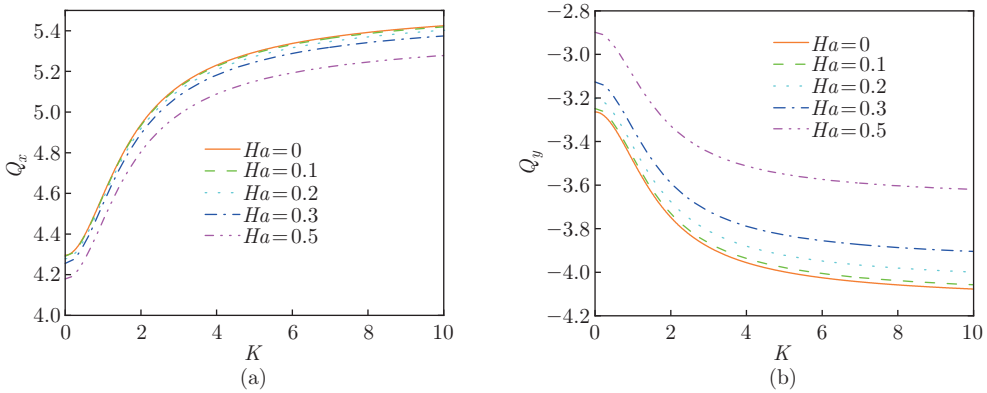

Fig. 11 Variations of the (a) Q_x-axial and (b) Q_y-transverse flow rates for diverse values of Ha when $\omega = 1$, $Re = 0.01$, $S = 0.5$, $J = 0.1$, $Pr = 21$, $\lambda = 10$, $\beta_1 = \beta_2 = 0.1$, and $\gamma = 3$ (color online)

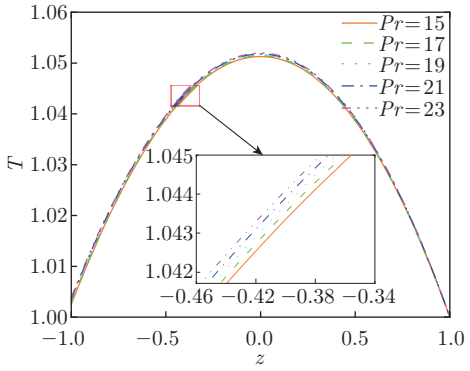

Fig. 12 Effects of Pr on the thermal distribution when $Re = 0.01$, $S = 0.5$, and $J = 0.1$ (color online)

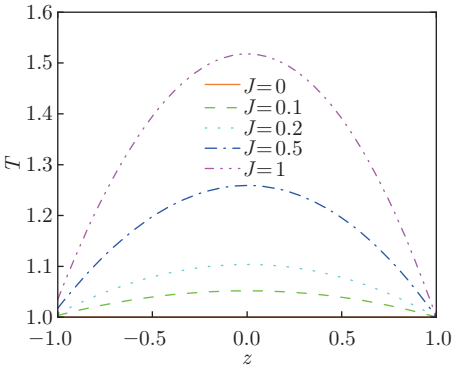

Fig. 13 Effects of J on the thermal distribution when $Re = 0.01$, $S = 0.5$, and $Pr = 21$ (color online)

4 Conclusions

In the present analysis, we have formulated a mathematical model to describe the thermal characteristics on the MHD and EOF of the couple stress fluid in a rotating microchannel under a slip boundary condition at both the walls. We obtain an exact solution for the temperature and velocity distributions inside the channel by using the Debye-Hückel linear approximation. Compared with the known analytical results for Newtonian fluid, the present theoretical analysis is proven to be effective and correct. The effects of several physical parameters are discussed thoroughly. In most cases, both velocity profiles achieve symmetrical distributions about the axis of the channel. The major outcomes of the current examination are outlined as follows.

(i) The MHD and axial EOF velocities decrease towards the central region of the flow domain for higher values of the rotational Reynolds number due to the Coriolis force effect. This phenomenon is due to the rotational effects of suppressing the axial velocity and elevating the transverse velocity.

(ii) The MHD and EOF velocity fields are remarkably affected by increasing the numerical values of the couple stress parameter. This is because both the electric force and the magnetic force drive the flow in both directions, as the couple stresses are continuously trying to oppose the microchannel fluid flow.

(iii) For higher values of the Hartmann number, the Lorentz force plays a more critical role in the fluid motion than the Coriolis force does. The Lorentz force creates a resistive force on the couple stress fluid in the channel, which retards the velocity in both the axial and the transverse directions.

(iv) The rotating MHD and EOF velocities increase with an enhancement in the buoyancy parameter due to the differences of gravity and temperature between the channel walls.

(v) The temperature of the fluid in a rotating microchannel increases with the Prandtl number and the Joule heating parameter.

The present investigation can be extended to include the steric and visco-electric effects on the EOF. Further, we would like to focus on the non-uniform zeta potential along the plates of the microchannel.

References

[1] GRAVESEN, P., BRANEBJERG, J., and JENSEN, O. S. Microfluidics — a review. *Journal of Micromechanics and Microengineering*, **3**, 168–182 (1993)

[2] BECKER, H. and GARTNER, C. Polymer microfabrication methods for microfluidic analytical applications. *Electrophoresis*, **21**, 12–26 (2000)

[3] ZIAIE, B., BALDI, A., LEI, M., GU, Y., and SIEGEL, R. A. Hard and soft micromachining for BioMEMS: review of techniques and examples of applications in microfluidics and drug delivery. *Advanced Drug Delivery Reviews*, **56**, 145–172 (2004)

[4] NGUYEN, N. T. and WU, Z. Micromixers — a review. *Journal of Micromechanics and Microengineering*, **15**, R1–R16 (2004)

[5] OHNO, K., TACHIKAWA, K., and MANZ, A. Microfluidics: applications for analytical purposes in chemistry and biochemistry. *Electrophoresis*, **29**, 4443–4453 (2008)

[6] STONE, H. A., STROOCK, A. D., and AJDARI, A. Engineering flows in small devices: microfluidics toward a lab-on-a-chip. *Annual Review of Fluid Mechanics*, **36**, 381–411 (2004)

[7] LASTER, D. J. and SANTIAGO, J. G. A review of micropumps. *Journal of Micromechanics and Microengineering*, **14**, R35–R64 (2004)

[8] MASLIYAH, J. and BHATTACHARJEE, S. *Electrokinetic and Colloid Transport Phenomena*, John Wiley and Sons, New Jersey (2006)

[9] KARNIADAKIS, G., BESKOK, A., and ALURU, N. *Microflows and Nanoflows*: *Fundamentals and Simulation*, Springer-Verlag, New York (2005)

[10] CHANG, C. and WANG, C. Rotating electro-osmotic flow over a plate or between two plates. *Physical Review E*, **84**, 056320 (2011)

[11] SI, D. Q., JIAN, Y. J., CHANG, L., and LIU, Q. S. Unsteady rotating electroosmotic flow through a slit microchannel. *Journal of Mechanics*, **32**, 603–611 (2016)

[12] GHESHLAGHI, B., NAZARIPOOR, H., KUMAR, A., and SADRZADEH, M. Analytical solution for transient electroosmotic flow in a rotating microchannel. *RSC Advances*, **6**, 17632–17641 (2016)

[13] ABHIMANYU, P., KAUSHIK, P., MONDAL, P. K., and CHAKRABORTY, S. Transiences in rotational electro-hydrodynamics microflows of a viscoelastic fluid under electrical double layer phenomena. *Journal of Non-Newtonian Fluid Mechanics*, **231**, 56–67 (2016)

[14] XIE, Z. Y. and JIAN, Y. J. Rotating electroosmotic flow of power-law fluids at high zeta potentials. *Colloids and Surfaces A*: *Physicochemical and Engineering Aspects*, **461**, 231–239 (2014)

[15] KAUSHIK, P., MANDAL, S., and CHAKRABORTY, S. Transient electroosmosis of a Maxwell fluid in a rotating microchannel. *Electrophoresis*, **38**, 2741–2748 (2017)

[16] LI, S. X., JIAN, Y. J., XIE, Z. Y., LIU, Q. S., and LI, F. Q. Rotating electro-osmotic flow of third grade fluids between two microparallel plates. *Colloids and Surfaces A*: *Physicochemical and Engineering Aspects*, **470**, 240–247 (2015)

[17] QI, C. and NG, C. O. Rotating electroosmotic flow of an Eyring fluid. *Acta Mechanica Sinica*, **33**, 295–315 (2017)

[18] SIVA, T., KUMBHAKAR, B., JANGILI, S., and MONDAL, P. K. Unsteady electro-osmotic flow of couple stress fluid in a rotating microchannel: an analytical solution. *Physics of Fluids*, **32**, 102013 (2020)

[19] LIU, Y. and JIAN, Y. Rotating electroosmotic flows in soft parallel plate microchannels. *Applied Mathematics and Mechanics* (*English Edition*), **40**(6), 1017–1028 (2019) https://doi.org/10.1007/s10483-019-2501-8

[20] LIU, Y. and JIAN, Y. Electromagnetohydrodynamic flows and mass transport in curved rectangular microchannels. *Applied Mathematics and Mechanics* (*English Edition*), **41**(9), 1431–1446 (2020) https://doi.org/10.1007/s10483-020-2649-9

[21] HAYAT, T., HAIDER, F., MUHAMMAD, T., and ALSAEDI, A. Darcy-Forchheimer flow by rotating disk with partial slip. *Applied Mathematics and Mechanics* (*English Edition*), **41**(5), 741–752 (2020) https://doi.org/10.1007/s10483-020-2608-9

[22] PATEL, M., KRUTHIVENTI, S. S. H., and KAUSHIK, P. Polyelectrolyte layer grafting effect on the rotational electroosmotic flow of viscoplastic material. *Microfluidics and Nanofluidics*, **25**, 11 (2021)

[23] JANG, J. and LEE, S. S. Theoretical and experimental study of MHD (magnetohydrodynamic) micropump. *Sensors and Actuators A*: *Physical*, **80**, 84–89 (2000)

[24] KIM, S. J. and KIM, D. Forced convection in microstructure for electronic equipment cooling. *ASME Journal of Heat Transfer*, **121**, 639–645 (1999)

[25] MUKHOPADHYAY, A., BANERJEE, S., and GUPTA, C. Fully developed hydrodynamic and thermal transport in combined pressure and electrokinetically driven flow in a microchannel with asymmetric boundary conditions. *International Journal of Heat and Mass Transfer*, **52**, 2145–2154 (2009)

[26] MAYNES, D. and WEBB, B. D. Fully developed electro-osmotic heat transfer in microchannels. *International Journal of Heat and Mass Transfer*, **46**, 1359–1369 (2003)

[27] HORIUCHI, K. and DUTTA, P. Joule heating effects in electroosmotically driven microchannel flows. *International Journal of Heat and Mass Transfer*, **47**, 3085–3095 (2004)

[28] SADEGHI, A. and SAIDI, M. H. Viscous dissipation effects on thermal transport characteristics of combined pressure and electroosmotically driven flow in microchannels. *International Journal of Heat and Mass Transfer*, **53**, 3782–3791 (2010)

[29] VAKILI, M. A., SAIDI, M. H., and SADEGHI, A. Thermal transport characteristics pertinent to electrokinetic flow of power-law fluids in rectangular microchannels. *International Journal of Thermal Sciences*, **79**, 76–89 (2014)

[30] KOO, J. and KLEINSTREUER, C. Viscous dissipation effects in microtubes and microchannels. *International Journal of Heat and Mass Transfer*, **47**, 3159–3169 (2004)

[31] STOKES, V. K. Couple stresses in fluids. *Physics of Fluids*, **9**, 1709–1715 (1966)

[32] NADUVINAMANI, N. B., HIREMATH, P. S., and GURUBASAVARAJ, G. Squeeze film lubrication of a short porous journal bearing with couple stress fluids. *Tribology International*, **34**, 739–747 (2001)

[33] ARIMAN, T. and CAKMAK, A. S. Couple stresses in fluids. *Physics of Fluids*, **10**, 2497–2499 (1967)

[34] STOKES, V. K. Effects of couple stresses in fluids on hydromagnetic channel flows. *Physics of Fluids*, **11**, 1131–1133 (1968)

[35] STOKES, V. K. *Theories of Fluids with Microstructure*: *an Introduction*, Springer-Verlag, New York (1984)

[36] DEVAKAR, M., SREENIVASU, D., and SHANKAR, B. Analytical solutions of couple stress fluid flows with slip boundary conditions. *Alexandria Engineering Journal*, **53**, 723–730 (2014)

[37] TRIPATHI, D., YADAV, A., and BEG, O. Electro-osmotic flow of couple stress fluids in a microchannel propagated by peristalsis. *The European Physical Journal Plus*, **132**, 173 (2017)

[38] MISRA, J. C. and CHANDRA, S. Effect of couple stresses on electrokinetic oscillatory flow of blood in the microcirculatory system. *Journal of Mechanics in Medicine and Biology*, **18**, 1850035 (2018)

[39] SINHA, A., MONDAL, A., SHIT, G. C., and KUNDU, P. K. Effect of heat transfer on rotating electroosmotic flow through a micro-vessel: haemodynamical applications. *Heat and Mass Transfer*, **52**, 1549–1557 (2015)

[40] SUN, R., HU, W., JIAO, B., and QI, C. Heat transfer characteristics and entropy generation of electroosmotic flow in a rotating rectangular microchannel. *International Journal of Thermal Sciences*, **140**, 238–254 (2019)

[41] LI, S. X., JAIN, Y. J., XIE, Z. Y., LIU, Q. S., and LI, F. Q. Rotating electroosmotic flow of third grade fluids between two microparallel plates. *Colloids and Surfaces A*: *Physicochemical and Engineering Aspects*, **470**, 240–247 (2015)

[42] GUILLERMO, I. Entropy generation in MHD porous channel with hydrodynamic slip and convective boundary conditions. *International Journal of Heat and Mass Transfer*, **80**, 274–280 (2015)

[43] GIREESHA, B., SRINIVAS, C., SHASHIKUMAR, N., MACHA, M., SIHGH, K., and MAHANTHESH, B. Entropy generation and heat transport analysis of Casson fluid flow with viscous and Joule heating in an inclined porous microchannel. *Journal of Process Mechanical Engineering*, **233**, 1173–1184 (2019)

[44] AWAN, A., ALI, M., and ABRO, K. Electroosmotic slip flow of Oldroyd-B fluid between two plates with non-singular kernel. *Journal of Computational and Applied Mathematics*, **376**, 112885 (2020)

[45] MONDAL, A., MANDAL, P. K., WEIGAND, B., and NAYAK, A. K. Entropic and heat-transfer analysis of EMHD flows with temperature-dependent properties. *Fluid Dynamics Research*, **52**, 065503 (2020)

[46] SUBRAMANIAM, C. G. and MONDAL, P. K. Effect of couple stresses on the rheology and dynamics of linear Maxwell viscoelastic fluids. *Physics of Fluids*, **32**, 013108 (2020)

[47] MONDAL, P. K. and WONGWISES, S. Magnetohydrodynamic (MHD) micropump of nanofluids in a rotating microchannel under electrical double-layer effect. *Journal of Process Mechanical Engineering*, **234**, 318–330 (2020)

[48] XIE, Z. Y., JAIN, Y. J., and LI, F. Q. Thermal transport of magnetohydrodynamic electroosmotic flow in circular cylindrical microchannels. *International Journal of Heat and Mass Transfer*, **119**, 355–364 (2018)

[49] JAIN, Y., SI, D., CHANG, L., and LIU, Q. Transient rotating electromagnetohydrodynamic micropumps between two infinite microparallel plates. *Chemical Engineering Science*, **134**, 12–22 (2015)